ISSN: 2476-6909; Modares. Mech. Eng. *2025;25(05):285-293.*

Modares Mechanical Engineering

DOI: 10.48311/MME.25.5.285
journal homepage: www.mme.modares.ac.ir

Enhanced Joint Coordinate Space Estimation for Precise Position Control of SCARA Robot under Parametric Uncertainty

Sina Dianat, Majid Sadedel*, Behzad Saeedi

Departmant of Mechanical Engineering, Tarbiat Modares University, Tehran, Iran

ARTICLE INFO

Article Type
Original Research

Article History
Received: November 09, 2024
Revised: May 20, 2025
Accepted: June 02, 2025
ePublished: August 12, 2025

ABSTRACT

In contemporary robotics, enhancing performance accuracy remains a critical and ongoing challenge. As robotic systems are increasingly utilized in precision-demanding applications such as surgical procedures and industrial welding, the demand for higher accuracy in end-effector positioning continues to grow. Numerous techniques have been proposed to address this issue. This study introduces a novel methodology that integrates the pseudo-inverse approach for error estimation—based on Taylor series expansion—with forward kinematics to extract uncertainty parameters. The refined inverse kinematics solutions, obtained through the Newton-Raphson method, are implemented on a SCARA robot for validation. The proposed approach yields substantial accuracy improvements, achieving a 99.8% enhancement in the x-direction and a 99.8% error reduction in the y-direction, thereby underscoring its potential for high-precision robotic applications.

Keywords: Accurate Position Control, SCARA Robot, Forward and Inverse Kinematics, Pseudo-Inverse, Taylor Expansion, Newton-Raphson Method

How to cite this article
Dianat S, Sadedel M, Saeedi B, Enhanced Joint Coordinate Space Estimation for Precise Position Control of SCARA Robot under Parametric Uncertainty. Modares Mechanical Engineering; *2025;25(05):285-293.*

*Corresponding author's email: majid.sadedel@modares.ac.ir
*Corresponding ORCID ID: 0000-0002-0285-8460

1- Introduction

1-1- State of the Art

The integration of robotic systems into a wide range of applications—from industrial automation to medical fields such as surgery and rehabilitation—has become increasingly essential [1–5]. However, during operation, robots are susceptible to various sources of error arising from both internal kinematic inaccuracies and external environmental disturbances, including noise, temperature variations, and load-induced effects [6]. In high-precision industrial tasks, robot accuracy is a critical performance metric, yet it may deteriorate under heavy payloads due to structural deformations [7]. Similarly, in medical robotics—particularly in surgical applications—the precise positioning and orientation of the end-effector are vital for ensuring safe and effective outcomes [8]. Enhancing robotic accuracy can be achieved by identifying and updating the physical parameters of the robot model embedded within its control system [9, 10]. While robotic manipulators are increasingly utilized in advanced applications such as robotic machining, laser welding, laser cutting, and coordinated multi-robot operations, they are often characterized by high repeatability but limited absolute accuracy. Therefore, to improve positioning precision, robotic systems typically require a thorough calibration process prior to deployment. Identifying kinematic errors during robot calibration typically necessitates experimental measurements of the end-effector's pose, encompassing both its three-dimensional position and orientation components [11]. Although robotic manipulators generally exhibit high repeatability, their absolute accuracy remains relatively low and has been extensively reported in the literature [12].

Studies have shown that the primary sources of inaccuracy stem from both geometric and non-geometric errors [13], [14]. Geometric errors originate from manufacturing tolerances, assembly misalignments, and structural inaccuracies. In contrast, non-geometric errors are attributed to factors such as elastic deformations, thermal effects, gear backlash, and interaction forces with the environment [15]. Fortunately, these errors can be mitigated through an effective calibration process. A successful calibration strategy relies on two fundamental components: constructing a precise kinematic model of the robot and utilizing a reliable method for accurately measuring the end-effector's pose during the calibration procedure [16, 17]

While several researchers, such as Marco Schiavon [18] have employed the conventional Denavit-Hartenberg (DH) model for robot calibration, this approach proves inadequate for robots featuring parallel arm configurations. To address this limitation, Hayati [19] introduced the Modified Denavit-Hartenberg (MDH) model, which offers greater flexibility for such kinematic structures. In addition to geometric modeling improvements, advanced calibration techniques—often referred to as third-level calibration—have also been explored. For example, Albert Nubiola [20], [21] incorporated the influence of temperature variations into the calibration process, enhancing the model's robustness under varying thermal conditions. Wang Zhenhua [22] proposed a novel calibration method that eliminates the need for constructing a base frame by utilizing distance error measurements from mobile robots. Furthermore, Zhu Jian [23] developed a gesture selection algorithm capable of identifying optimal configurations from a large set of pre-measured poses, thereby mitigating the risk of local convergence during calibration.

Another source of uncertainty commonly observed in robotic joints is clearance joints. These represent inherent nonlinearities in space mechanisms that significantly impact the system's dynamic behavior and increase its sensitivity to parameter variations. The interaction between joint clearances and parameter uncertainties poses a major challenge, as it degrades both the kinematic accuracy and dynamic performance of space robotic manipulators. In this context, Wuweikai Xiang [24] investigated the dynamic behavior of space manipulators by simultaneously accounting for joint clearance and parameter uncertainty, modeling the joints as contact-collision elements. To further elucidate the relationship between system parameters and dynamic response, the Chebyshev polynomial method was employed [25]. This approach enables the evaluation of the dynamic response of uncertain mechanisms through interval-based algorithms. Additionally, a sensitivity analysis method was incorporated to reduce the influence of parameter fluctuations and enhance the robustness of the system's performance.

Further investigations into the dynamics of space robotic manipulators under joint clearance and parameter uncertainty have explored the effects of clearance size and friction coefficients, both as individual and combined uncertain parameters. These studies quantitatively evaluated how such uncertainties influence the dynamic response of the manipulator, providing deeper insight into the system's sensitivity. The findings offer valuable contributions to the design, analysis, and validation of space robotic manipulators by highlighting the critical importance of accounting for both clearance effects and parametric uncertainties to ensure reliable performance in space environments.

Based on the literature reviewed in this study, numerous research efforts have been dedicated to enhancing the accuracy and performance of robotic systems. Qingxing Meng [26] presents a comprehensive control strategy for a two-link rigid–flexible manipulator, emphasizing precise position control while managing vibration constraints. This integrated solution includes motion planning and adaptive tracking, utilizing advanced techniques such as virtual damping, online trajectory correction, radial basis function neural networks, and sliding mode control. The methodology shows significant improvements in handling the inherent uncertainties of robotic systems, as demonstrated by robust simulation results. Ryan L. Truby [27] offers a pioneering framework for proprioceptive perception in soft robotics, utilizing a kirigami-inspired sensorization technique combined with deep learning algorithms. This research advances the understanding of soft robot geometry and kinematics, using recurrent neural networks to address the challenges posed by non-linear sensor feedback. The successful implementation on a soft robotic arm equipped with a complex array of actuators and sensors highlights the approach's viability, paving the way for sophisticated closed-loop control systems in soft robotics. Jiehao Li [28], in exploring parallel mechanisms for wheel-legged robots, introduces a neural fuzzy-based model predictive tracking scheme (NFMPC) to tackle the challenges of accurate trajectory tracking and stable heavy-load operation in complex environments. The study showcases the BIT-NAZA robot, demonstrating the hybrid control strategy's effectiveness in maintaining stability and tracking precision despite unpredictable disturbances and nonlinearities. These findings provide substantial theoretical and practical insights, potentially guiding the future development of intelligent robotic systems with enhanced lateral stability [29, 30]

The literature reviewed here mentions only a limited number of studies on the accuracy and behavior of robot end-effectors. Therefore, a more comprehensive analysis can be conducted by examining additional sources [31–35].

1-2- Contribution

Despite the extensive body of research on robotic calibration and accuracy enhancement, current methodologies often exhibit limitations in adaptability, analytical efficiency, or generalizability across different robot architectures. In particular, few studies provide a unified analytical framework that addresses both error estimation and inverse kinematics refinement, especially under uncertainty conditions.

This study addresses these limitations by introducing a novel mathematical approach that combines pseudo-inverse analysis with Taylor series expansion and Newton-Raphson-based inverse kinematics refinement. The key contributions are summarized as follows:

- Identification of a methodological gap in addressing configuration uncertainties within inverse kinematics, particularly for SCARA-type robotic systems.
- Development of an integrated approach using the pseudo-inverse method for analytical estimation of kinematic errors.
- Application of Taylor series expansion to linearize nonlinear kinematic relationships for improved tractability and error propagation analysis.
- Refinement of inverse kinematics solutions through iterative Newton-Raphson methods, enhancing convergence stability and model robustness.
- Formulation of a computationally efficient framework that supports implementation in high-precision applications without reliance on data-intensive learning models.

This contribution offers a structured and adaptable solution to improving robotic accuracy in systems where analytical transparency and real-time performance are essential.

1-3- Outline

The remainder of this paper is organized as follows: Section 2 presents the kinematic and dynamic modeling of the SCARA robot in an ideal environment. Section 3 introduces the modeling of joint uncertainties and their effects on robot performance. Section 4 details the estimation of uncertainty parameters. Section 5 addresses joint space estimation and precise end-effector control. Section 6 presents and discusses the results. Finally, Section 7 concludes the study and outlines future directions.

2- Modeling SCARA Robot Kinematics in an Idealized Environment

The SCARA robot is a robot with three degrees of freedom. As shown in Figure 1a, the movement of this robot consists of two consecutive rotations followed by one prismatic. Generally, errors are generated for the rotational joints. Considering that the movement of the robot's last link is prismatic, the robot's movement will be examined up to this translation. Figure 1b shows the top view of the three-dimensional model, which includes two rotations around the z-axis.

In ideal mode, link (1) rotates around z_0 in the zero coordinate system with the angle θ_1 and link (2) rotates around z_1 with the angle θ_2. The ideal model of the robot includes rotation in the direction of z_0 by the angle of the first link (θ_1) and rotation in the direction of z_1 by the angle of the second link (θ_2). Therefore, considering the importance of examining the end-effector's position in the ideal state, we need to analyze the workspace of the robot presented in Figure 1. For this task, we can use transformation matrix that transforms one vector into another vector by the process of matrix multiplication. The transformation matrix alters the cartesian system and maps the coordinates of the vector to the new coordinates. The transformation matrix of transfer in the direction of the x, y and z axes is calculated from equations (1), (2) and (3) respectively.

$$T_p^x(P_x) = \begin{bmatrix} 1 & 0 & 0 & P_x \\ 0 & 1 & 0 & 0 \\ 0 & 0 & 1 & 0 \\ 0 & 0 & 0 & 1 \end{bmatrix} \quad (1)$$

$$T_p^y(P_y) = \begin{bmatrix} 1 & 0 & 0 & 0 \\ 0 & 1 & 0 & P_x \\ 0 & 0 & 1 & 0 \\ 0 & 0 & 0 & 1 \end{bmatrix} \quad (2)$$

$$T_p^z(P_z) = \begin{bmatrix} 1 & 0 & 0 & 0 \\ 0 & 1 & 0 & 0 \\ 0 & 0 & 1 & P_z \\ 0 & 0 & 0 & 1 \end{bmatrix} \quad (3)$$

The transformation matrix of rotation in the direction of the x, y and z axes is calculated from equations (4), (5) and (6) respectively.

$$T_r^x(\alpha) = \begin{bmatrix} 1 & 0 & 0 & 0 \\ 0 & cos(\alpha) & -sin(\alpha) & 0 \\ 0 & sin(\alpha) & cos(\alpha) & 0 \\ 0 & 0 & 0 & 1 \end{bmatrix} \quad (4)$$

$$T_r^y(\beta) = \begin{bmatrix} cos(\beta) & 0 & sin(\beta) & 0 \\ 0 & 1 & 0 & 0 \\ -sin(\beta) & 0 & cos(\beta) & 0 \\ 0 & 0 & 0 & 1 \end{bmatrix} \quad (5)$$

$$T_r^z(\gamma) = \begin{bmatrix} cos(\gamma) & -sin(\gamma) & 0 & 0 \\ sin(\gamma) & cos(\gamma) & 0 & 0 \\ 0 & 0 & 1 & 0 \\ 0 & 0 & 0 & 1 \end{bmatrix} \quad (6)$$

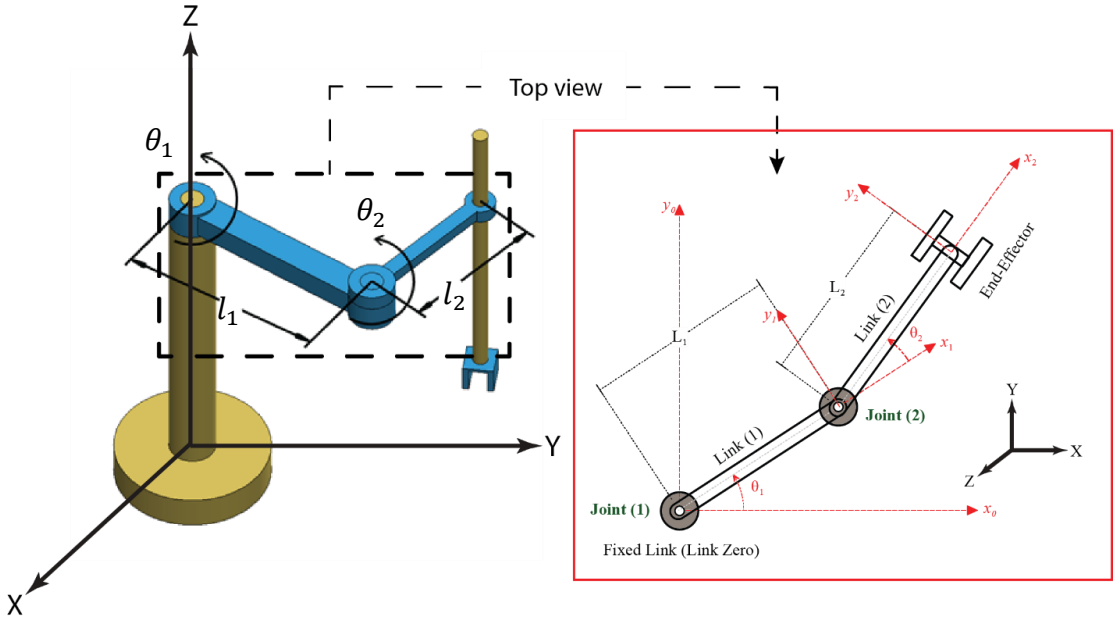

a) SCARA Robot 3D Model

b) Top view (Ideal Model)

Fig.1 SCARA Robot Model

Therefore, the transformation matrix that shows the location of the end-effector relative to the primary inertia frame coordinate system (the zero-coordinate system) can be calculated as follows.

$$T_{ideal} = T_r^z(\theta_1)T_p^x(l_1)T_r^z(\theta_2)T_p^x(l_2) = \begin{bmatrix} C(\theta_1+\theta_2) & -S(\theta_1+\theta_2) & 0 & l_1C(\theta_1)+l_2C(\theta_1+\theta_2) \\ S(\theta_1+\theta_2) & C(\theta_1+\theta_2) & 0 & l_1S(\theta_1)+l_2S(\theta_1+\theta_2) \\ 0 & 0 & 1 & 0 \\ 0 & 0 & 0 & 1 \end{bmatrix} \quad (7)$$

According to equation (7), the displacement values in the x and y directions for the end-effector in the ideal state can be extracted from end column, which are calculated from equations (8) and (9).

$$x_{ideal} = l_1 Cos(\theta_1) + l_2 Cos(\theta_1+\theta_2) \quad (8)$$

$$y_{ideal} = l_1 Sin(\theta_1) + l_2 Sin(\theta_1+\theta_2) \quad (9)$$

Based on the above equation, the workspace of the robot in an ideal state, considering the range of motion from $-\frac{\pi}{2}rad$ to $\frac{\pi}{2}rad$ for joint number one and from $-\frac{3\pi}{4}rad$ to $\frac{3\pi}{4}rad$ for joint number tow, is illustrated in Figure 3.

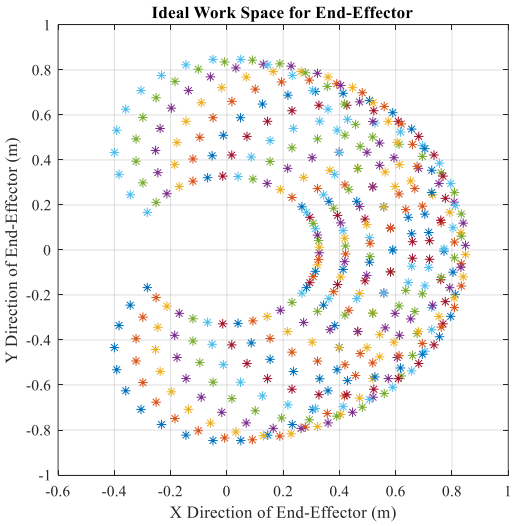

Fig. 2 Robot Worlspace in Ideal State

3- Modeling the Robot's Performance by Taking into Account the Uncertainty in the Joints

To model the robot by taking into account the uncertainty, error parameters are introduced. In general and regardless of the factors causing the errors, the error can be considered as three translations and three rotations in the direction of x, y and z. The rotations are considered as Euler angles. The sum of these six DOFs expresses a complete model of the types of errors, which we call the error model. To express all the robot's errors, the error model must be placed between the ground and the first link (on the first joint) and between the first link and the second link (on the second joint). Considering that the two-link robot moves in the plane, one can ignore the rotation errors in the direction of x and y and the translation in the direction of z. Because these errors have no effect on the displacement (in the two directions of x and y) of the end-effector. Therefore, the transformation matrix of the error model is calculated from equation (10).

$$T_{err} = T_p^x(\varepsilon_x)T_p^y(\varepsilon_y)T_r^z(\varepsilon_\theta) \quad (10)$$

The transformation matrix of the non-ideal model is also calculated from equation (11).

$$T_{non-ideal} = T_{err_1}T_r^z(\theta_1)T_p^x(l_1)T_{err_2}T_r^z(\theta_2)T_p^x(l_2) = \begin{bmatrix} T_{11} & T_{12} & 0 & T_{14} \\ T_{21} & T_{22} & 0 & T_{24} \\ 0 & 0 & 1 & 0 \\ 0 & 0 & 0 & 1 \end{bmatrix} \quad (11)$$

Where:

$$\begin{aligned} T_{11} &= Cos(\varepsilon_{\theta_1}+\theta_1+\theta_2+\varepsilon_{\theta_2}) \\ T_{12} &= -Sin(\varepsilon_{\theta_1}+\theta_1+\theta_2+\varepsilon_{\theta_2}) \\ T_{14} &= \varepsilon_{x_1} + l_1C(\varepsilon_{\theta_1}+\theta_1) + \varepsilon_{x_2}C(\varepsilon_{\theta_1}+\theta_1) - \\ &\quad \varepsilon_{y_2}S(\varepsilon_{\theta_1}+\theta_1) + l_2C(\varepsilon_{\theta_1}+\theta_1+\theta_2+\varepsilon_{\theta_2}) \\ T_{21} &= Sin(\varepsilon_{\theta_1}+\theta_1+\theta_2+\varepsilon_{\theta_2}) \\ T_{22} &= Cos(\varepsilon_{\theta_1}+\theta_1+\theta_2+\varepsilon_{\theta_2}) \\ T_{24} &= \varepsilon_{y_1} + l_1S(\varepsilon_{\theta_1}+\theta_1) + \varepsilon_{x_2}S(\varepsilon_{\theta_1}+\theta_1) + \\ &\quad \varepsilon_{y_2}C(\varepsilon_{\theta_1}+\theta_1) + l_2S(\varepsilon_{\theta_1}+\theta_1+\theta_2+\varepsilon_{\theta_2}) \end{aligned} \quad (12)$$

According to equation (11), the displacement values in the x and y directions for the end-effector in the non-ideal state can be extracted from end column, which are calculated from equations (12) and (13).

$$x_{non-ideal} = T_{14} \quad (13)$$

$$y_{non-ideal} = T_{24} \quad (14)$$

The displacement error values in the x and y directions are also calculated from equations (14) and (15).

$$E_x = x_{ideal} - x_{non-ideal} = \varepsilon_{y_2}S(\varepsilon_{\theta_1}+\theta_1) - \varepsilon_{x_2}C(\varepsilon_{\theta_1}+\theta_1) - l_1C(\varepsilon_{\theta_1}+\theta_1) - \varepsilon_{x_1} + l_2C(\varepsilon_{\theta_1}+\theta_1) + l_1C(\theta_1) - l_2C(\varepsilon_{\theta_1}+\theta_1+\theta_2+\varepsilon_{\theta_2}) \quad (15)$$

$$E_y = y_{ideal} - y_{non-ideal} = l_2S(\theta_1+\theta_2) - \varepsilon_{y_2}C(\varepsilon_{\theta_1}+\theta_1) - \varepsilon_{x_2}S(\varepsilon_{\theta_1}+\theta_1) - l_1S(\theta_1+\theta_2) - \varepsilon_{y_1} + l_1S(\theta_1) - l_2S(\varepsilon_{\theta_1}+\theta_1+\theta_2+\varepsilon_{\theta_2}) \quad (16)$$

According to Figure 4, the non-ideal model of the robot includes the error model between the ground and the first link, rotation in the direction of z_2 by the angle of the first link (θ_1), the error model between the first and the second link, and rotation in the direction of z_6 by the angle of the second link (θ_2).

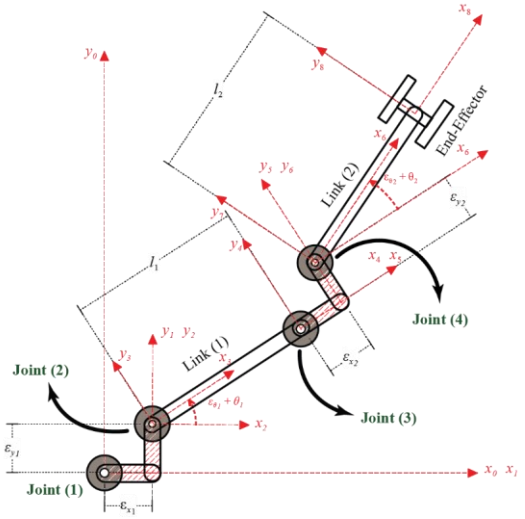

Fig. 3 Non-ideal Model

4- Calculation of Uncertainty Parameters

To calculate the error parameters, using the Taylor expansion up to the first order, they can be approximated to an acceptable value. For this purpose, based on the non-ideal robot model that has 6 error components, the displacement errors in the x and y directions of the robot's end-effector are calculated. Then, considering the smallness of the error components and using the first-order Taylor expansion, a first-order approximation of these errors is calculated. As stated, the displacement error values in the x and y directions are also calculated

from equations (14) and (15). According to the Taylor expansion for each of the errors, one can write:

$$E \approx C_0 + C_1\varepsilon_{x_1} + C_2\varepsilon_{y_1} + C_3\varepsilon_{\theta_1} + C_4\varepsilon_{x_2} + C_5\varepsilon_{y_2} + C_6\varepsilon_{\theta_2} \quad (17)$$

The unknown coefficients of equation (16) are functions of θ_1 and θ_2 and calculate as follows:

$$C_0 = E|_{\varepsilon_{x_1},\varepsilon_{y_1},\varepsilon_{\theta_1},\varepsilon_{x_2},\varepsilon_{y_2},\varepsilon_{\theta_2}=0} \quad (18)$$

$$C_1 = \left.\frac{\partial E}{\partial \varepsilon_{x_1}}\right|_{\varepsilon_{x_1},\varepsilon_{y_1},\varepsilon_{\theta_1},\varepsilon_{x_2},\varepsilon_{y_2},\varepsilon_{\theta_2}=0} \quad (19)$$

$$C_2 = \left.\frac{\partial E}{\partial \varepsilon_{y_1}}\right|_{\varepsilon_{x_1},\varepsilon_{y_1},\varepsilon_{\theta_1},\varepsilon_{x_2},\varepsilon_{y_2},\varepsilon_{\theta_2}=0} \quad (20)$$

$$C_3 = \left.\frac{\partial E}{\partial \varepsilon_{\theta_1}}\right|_{\varepsilon_{x_1},\varepsilon_{y_1},\varepsilon_{\theta_1},\varepsilon_{x_2},\varepsilon_{y_2},\varepsilon_{\theta_2}=0} \quad (21)$$

$$C_4 = \left.\frac{\partial E}{\partial \varepsilon_{x_2}}\right|_{\varepsilon_{x_1},\varepsilon_{y_1},\varepsilon_{\theta_1},\varepsilon_{x_2},\varepsilon_{y_2},\varepsilon_{\theta_2}=0} \quad (22)$$

$$C_5 = \left.\frac{\partial E}{\partial \varepsilon_{y_1}}\right|_{\varepsilon_{x_1},\varepsilon_{y_1},\varepsilon_{\theta_1},\varepsilon_{x_2},\varepsilon_{y_2},\varepsilon_{\theta_2}=0} \quad (23)$$

$$C_6 = \left.\frac{\partial E}{\partial \varepsilon_{\theta_2}}\right|_{\varepsilon_{x_1},\varepsilon_{y_1},\varepsilon_{\theta_1},\varepsilon_{x_2},\varepsilon_{y_2},\varepsilon_{\theta_2}=0} \quad (24)$$

The above coefficients for the displacement error in the x direction are as follows:

$$C_0 = 0 \quad (25)$$

$$C_1 = -1 \quad (26)$$

$$C_2 = 0 \quad (27)$$

$$C_3 = \frac{2sin(\theta_1+\theta_2)}{5} + \frac{9sin(\theta_1)}{20} \quad (28)$$

$$C_4 = -1 \quad (29)$$

$$C_5 = 0 \quad (30)$$

$$C_6 = \frac{2sin(\theta_1+\theta_2)}{5} \quad (31)$$

The coefficients for the displacement error in the y direction are similarly as follows:

$$C_0 = 0 \quad (32)$$

$$C_1 = 0 \quad (33)$$

$$C_2 = -1 \quad (34)$$

$$C_3 = -\frac{2\,cos(\theta_1+\theta_2)}{5} - \frac{9cos(\theta_1)}{20} \quad (35)$$

$$C_4 = 0 \quad (36)$$

$$C_5 = -1 \quad (37)$$

$$C_6 = -\frac{2\,cos(\theta_1+\theta_2)}{5} \quad (38)$$

5- Estimation of Joint Space and Precise Control of Robot End-Effector Position

To find the robot's workspace in the ideal state, one must know the rotation range and the length of the links. These parameters are used according to Table 1.

Table 1 The range of rotation and length of links

Number of links	Range of rotation (rad)	Range of length (m)
1	$\left[-\frac{\pi}{2},\frac{\pi}{2}\right]$	**0.45**
2	$\left[-\frac{3\pi}{4},\frac{3\pi}{4}\right]$	**0.40**

To find the robot's workspace in the non-ideal state, one needs to first calculate the uncertainty parameters. According to the relation, one can write the uncertainty for the two directions of x and y for some points as follows:

$$\begin{bmatrix} E_x^1 \\ E_x^2 \\ \vdots \\ E_x^n \end{bmatrix} = \begin{bmatrix} -1 & \frac{2sin(\theta_1^1+\theta_2^1)}{5}+\frac{9sin(\theta_1^1)}{20} & -1 & \frac{2sin(\theta_1^1+\theta_2^1)}{5} \\ -1 & \frac{2sin(\theta_1^2+\theta_2^2)}{5}+\frac{9sin(\theta_1^2)}{20} & -1 & \frac{2sin(\theta_1^2+\theta_2^2)}{5} \\ \vdots & \vdots & \vdots & \vdots \\ -1 & \frac{2sin(\theta_1^n+\theta_2^n)}{5}+\frac{9sin(\theta_1^n)}{20} & -1 & \frac{2sin(\theta_1^n+\theta_2^n)}{5} \end{bmatrix} \begin{bmatrix} \varepsilon_{x_1} \\ \varepsilon_{\theta_1} \\ \varepsilon_{x_2} \\ \varepsilon_{\theta_2} \end{bmatrix} \quad (39)$$

$$\begin{bmatrix} E_y^1 \\ E_y^2 \\ \vdots \\ E_y^n \end{bmatrix} = \begin{bmatrix} -1 & -\frac{2\,cos(\theta_1^1+\theta_2^1)}{5}-\frac{9cos(\theta_1^1)}{20} & -1 & -\frac{2cos(\theta_1^1+\theta_2^1)}{5} \\ -1 & -\frac{2cos(\theta_1^2+\theta_2^2)}{5}-\frac{9cos(\theta_1^2)}{20} & -1 & -\frac{2cos(\theta_1^2+\theta_2^2)}{5} \\ \vdots & \vdots & \vdots & \vdots \\ -1 & -\frac{2cos(\theta_1^n+\theta_2^n)}{5}-\frac{9cos(\theta_1^n)}{20} & -1 & -\frac{2cos(\theta_1^n+\theta_2^n)}{5} \end{bmatrix} \begin{bmatrix} \varepsilon_{y_1} \\ \varepsilon_{\theta_1} \\ \varepsilon_{y_2} \\ \varepsilon_{\theta_2} \end{bmatrix} \quad (40)$$

In equations (38) and (39), the uncertainty parameters are on the right side. In each of these relations, there are n equations and 4 unknowns. For a simpler expression, one can rewrite the above equations as follows:

$$E_{x_{n\times1}} = C_{x_{n\times4}}\,\varepsilon_{x_{4\times1}} \quad (41)$$

$$E_{y_{n\times1}} = C_{y_{n\times4}}\,\varepsilon_{y_{4\times1}} \quad (42)$$

Considering that the number of equations is more than the number of unknowns, one can use the pseudo-inverse method [36] to obtain the unknowns.

$$\begin{aligned} &E_{n\times1} = C_{n\times4}\varepsilon_{4\times1} \\ &C_{4\times n}^T E_{n\times1} = C_{4\times n}^T C_{n\times4}\varepsilon_{4\times1} \end{aligned} \quad (43)$$

Where $C_{4\times n}^T$ is transpose on C. In above equation, $C_{4\times n}^T C_{n\times4}$ is a square matrix so can calculate inverse of it.

$$\begin{aligned} &(C_{4\times n}^T C_{n\times4})^{-1} C_{4\times n}^T E_{n\times1} = \varepsilon_{4\times1} \\ &Pinv(C_{n\times4}) = (C_{4\times n}^T C_{n\times4})^{-1} C_{4\times n}^T \\ &\varepsilon_{4\times1} = Pinv(C_{n\times4}) E_{n\times1} \end{aligned} \quad (44)$$

To calculate the uncertainty parameters, one needs experimental data. Due to the unavailability of the robot, one can assume some values for the uncertainty and then obtain hypothetical experimental data. The calculation of the assumed uncertainty parameters in this research is shown in Table 2.

Table 2 Assumed uncertainty parameters

Uncertainty parameter	Amount
ε_{x_1}	$\mathbf{0.001\ m}$
ε_{y_1}	$\mathbf{0.002\ m}$
ε_{θ_1}	$\mathbf{0.1\ rad}$
ε_{x_2}	$\mathbf{0.005\ m}$
ε_{y_2}	$\mathbf{0.003\ m}$
ε_{θ_2}	$\mathbf{0.07\ rad}$

Now one can solve equations (40) and (41) and calculate the uncertainty parameters. The spatial position of the robot end-effector in the non-ideal state can be calculated from equations (44) and (45) according to the inverse kinematics.

$$x_{non-ideal} = \varepsilon_{x_1} + l_1\,cos(\theta_1+\varepsilon_{\theta_1}) + \varepsilon_{x_2} + l_2\,cos(\theta_1+\varepsilon_{\theta_1}+\theta_2+\varepsilon_{\theta_2}) \quad (45)$$

$$y_{non-ideal} = \varepsilon_{y_1} + l_1\,sin(\theta_1+\varepsilon_{\theta_1}) + \varepsilon_{y_2} + l_2\,sin(\theta_1+\varepsilon_{\theta_1}+\theta_2+\varepsilon_{\theta_2}) \quad (46)$$

To precisely control the position of the robot end-effector by taking into account the uncertainty parameters, one must equate equations (42) and (43) with the position of the robot end-effector in the non-ideal state. As a result, for each point in the robot's workspace, a system of equations with two nonlinear equations and two unknowns that include θ_1 and θ_2 is formed. To solve this system of equations, one can use the Newton-Raphson method. By solving this system of equations, the values of θ_1 and θ_2 required for placing the robot end-

effector by taking into account the uncertainty parameters in the desired position will be obtained. As a result, one can precisely control the position of the robot end-effector.

6-Results and Discussion

According to Figure 4, it can be seen that the spatial position of the robot end-effector in the non-ideal state has a significant difference with the ideal state. The points that are shown with stars indicate the position of the end-effector in the ideal state and the points that are shown with circles indicate the position of the end-effector in the non-ideal state. For example, it can be seen that the spatial position of a point in the ideal state in the direction of the x-axis is 0.62 meters, while the position of the same point in the non-ideal state in the direction of the x-axis is 0.66 meters.

Figure 5 shows the displacement error in the x direction before and after compensation. The displacement error is also plotted as a function of the different joint angles and as a diagram for 36 points. At the top left, error of x direction befor compensation shown thas is in order of $10^{-2}m$ (centemeter). After compensation this error comes to order of $10^{-3}m$ (milimeter) that shown at top right. For showing more detaitls, there are tow figures that showes error of x direction fore a point in the same and different scales at the bottom according to this figure, the displacement error in the x direction has been significantly reduced after compensation. The results show that the accuracy in the x direction improved by 99.8%.

The comparison of the displacement error in the y direction, before and after compensation, is shown in Figure 6. The displacement error is also plotted as a function of the different joint angles and as a diagram for 36 points. At the top left, error of y direction befor compensation shown thas is in order of $10^{-2}m$ (centemeter). After compensation this error comes to order of $10^{-3}m$ (milimeter) that shown at top right. For showing more detaitls, there are tow figures that showes error of y direction fore a point in the same and different scales at the bottom according to this figure, the compensator has improved the accuracy in the y direction by 99.8%.

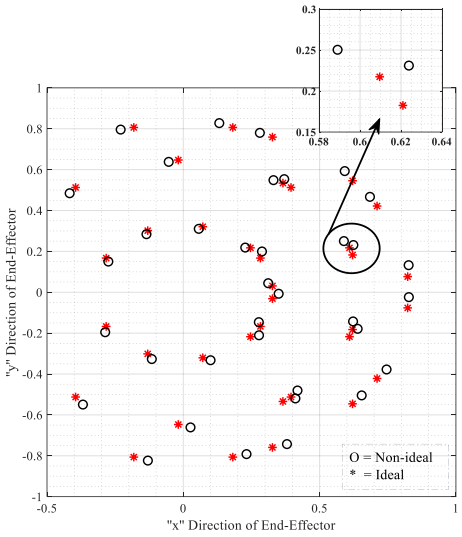

Fig. 4 Comparison of the position of the robot worker in ideal and non-ideal state

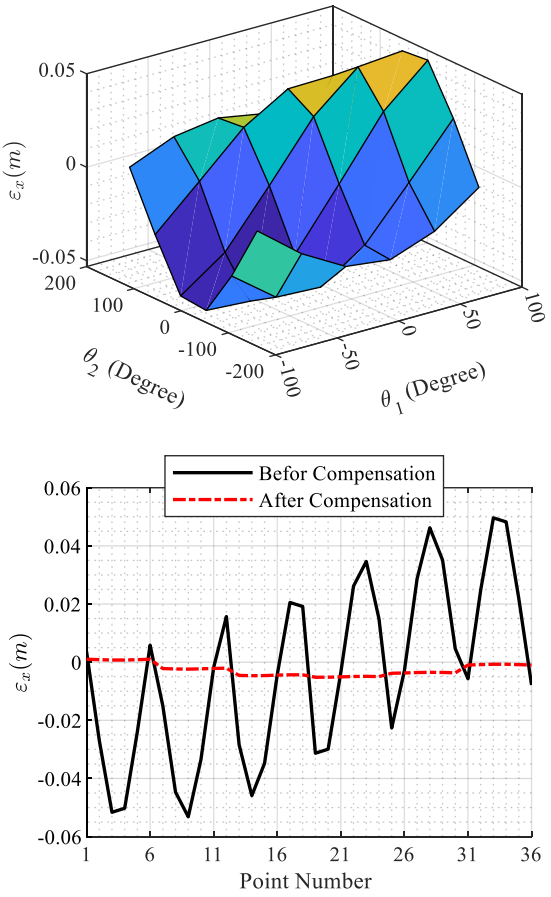

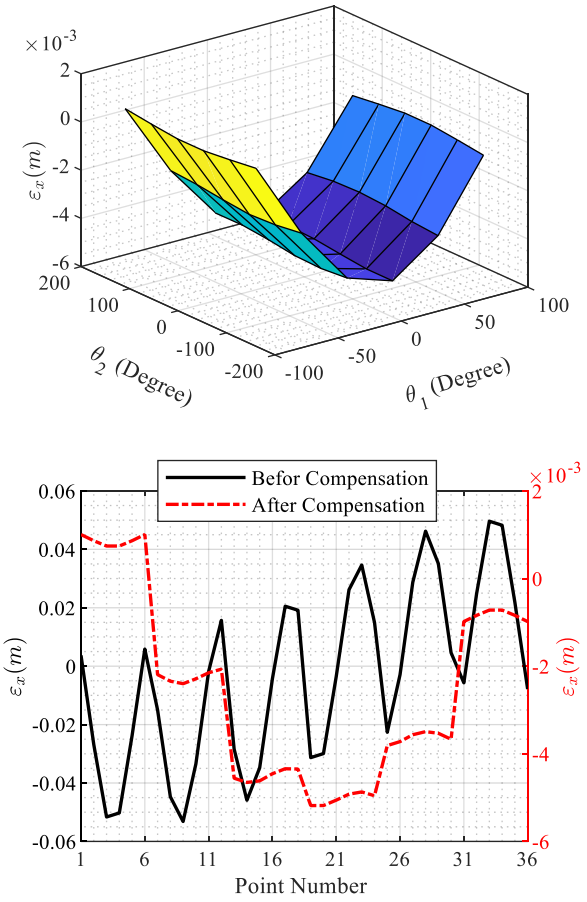

Fig.5 Displacement error in x direction before and after compensation

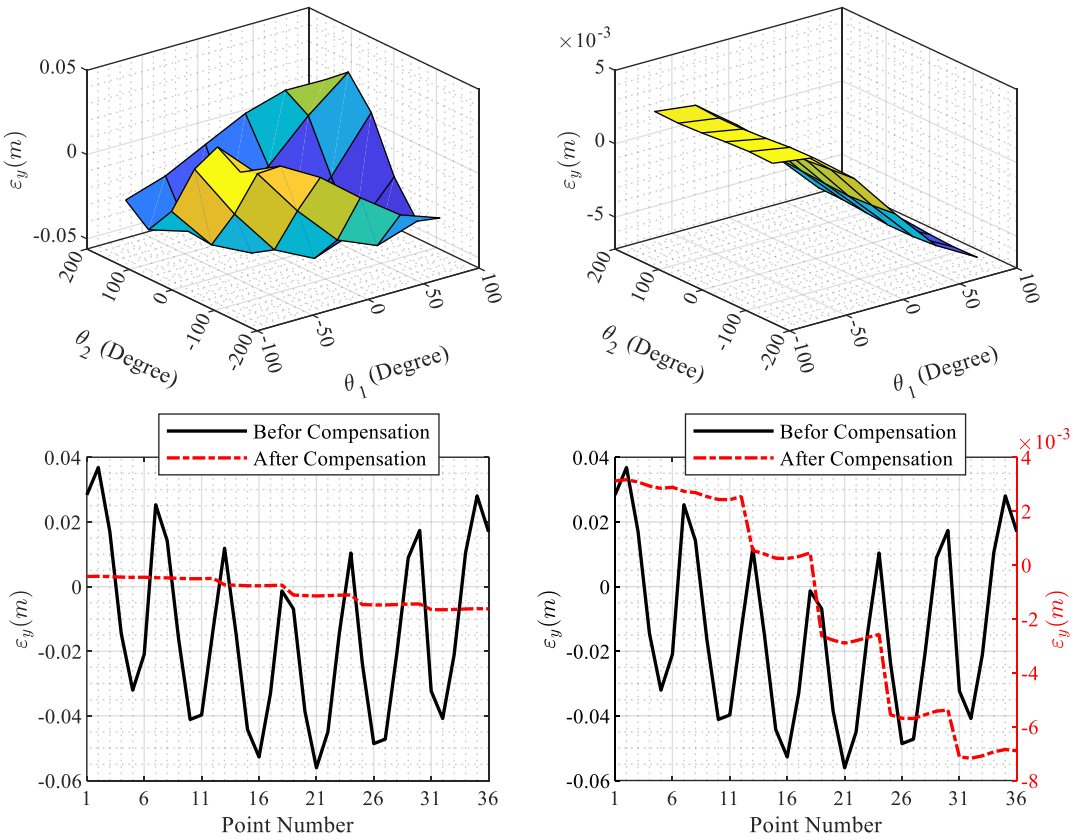

Fig.6 Displacement error in y direction before and after compensation

7-Conclusion

This research addresses the critical challenge of error compensation in robotic systems, which is essential for precision-demanding tasks such as welding and surgical operations. A novel approach was developed to reduce positional inaccuracies of the SCARA robot's end-effector by integrating joint uncertainties into the modeling framework. The method relies on a robust mathematical model, using forward kinematics to determine the ideal end-effector position and systematically quantifying deviations through first-order Taylor expansion and the Pseudo-inverse technique. Error correction was effectively achieved by applying the Newton-Raphson method combined with inverse kinematics. Although the analysis was conducted without physical robot experiments—relying on kinematic simulations and assumed errors—the proposed framework offers a practical foundation that can be experimentally validated when hardware becomes available. To enhance accuracy further, future studies could extend the error estimation using higher-order Taylor expansions and implement the method in real-world robotic systems. Overall, this study advances the understanding of error compensation in SCARA robots and provides a scalable methodology applicable to a broad range of robotic platforms requiring enhanced precision.

Ethical Statement: The content of this manuscript is original, based on the authors' research, and has not been published or submitted elsewhere, either in Iranian or international journals.

Competing interests: Not applicable.

Authors' contributions: All authors contributed to the study conception and design. Material preparation, data collection and analysis were performed by Sina Dianat, Majid Sadedel and Behzad Saeedi. The first draft of the manuscript was written by Sina Dianat and all authors commented on previous versions of the manuscript. All authors read and approved the final manuscript..

Funding: Not applicable.

Refrences

[1] M. Dehghani, M. Mohammadi Moghadam, and P. Torabi, "Analysis, optimization and prototyping of a parallel RCM mechanism of a surgical robot for craniotomy surgery," Industrial Robot: An International Journal, vol. 45, no. 1, pp. 78–88, Jan. 2018, doi: 10.1108/IR-08-2017-0144.

[2] M. Dehghani, R. A. McKenzie, R. A. Irani, and M. Ahmadi, "Robot-mounted sensing and local calibration for high-accuracy manufacturing," Robot Comput Integr Manuf, vol. 79, p. 102429, Feb. 2023, doi: 10.1016/j.rcim.2022.102429.

[3] B. Saeedi, M. Mohammadi Moghaddam, and M. Sadedel, "Inverse kinematics analysis of a wrist rehabilitation robot using artificial neural network and adaptive Neuro-Fuzzy inference system," Mechanics Based Design of Structures and Machines, pp. 1–49, May 2024, doi: 10.1080/15397734.2024.2356066.

[4] P.-N. Le and H.-J. Kang, "A New Manipulator Calibration Method for the Identification of Kinematic and Compliance Errors Using Optimal Pose Selection," Applied Sciences, vol. 12, no. 11, p. 5422, May 2022, doi: 10.3390/app12115422.

[5] B. Saeedi, M. Sadedel, and M. Mohammadi Moghaddam, "Innovative Integration of Meta-Heuristic Algorithms with Adaptive TSK Fuzzy Systems for Inverse Kinematics in a New Wrist and Forearm Rehabilitation Exoskeleton," Iranian Journal of Science and Technology - Transactions of Mechanical Engineering, vol. 49, no. 2,

pp. 927–962, Apr. 2025, doi: 10.1007/S40997-024-00811-9/METRICS.
[6] S. Asif and P. Webb, “Realtime Calibration of an Industrial Robot,” Applied System Innovation, vol. 5, no. 5, p. 96, Sep. 2022, doi: 10.3390/asi5050096.
[7] H. Yu, Q. Sun, C. Wang, and Y. Zhao, “Frequency response analysis of heavy-load palletizing robot considering elastic deformation,” Sci Prog, vol. 103, no. 1, p. 003685041989385, Jan. 2020, doi: 10.1177/0036850419893856.
[8] F. Cepolina and R. Razzoli, “Review of robotic surgery platforms and end effectors,” J Robot Surg, vol. 18, no. 1, p. 74, Feb. 2024, doi: 10.1007/s11701-023-01781-x.
[9] H.-N. Nguyen, T.-H. Nguyen, D.-T. Vo, and Q.-P. Pham, “MODEL BASED ROBOT CALIBRATION TECHNIQUE WITH CONSIDERATION OF JOINT COMPLIANCE,” Journal of Technology & Innovation, vol. 1, no. 1, pp. 06–09, Mar. 2021, doi: 10.26480/jtin.01.2021.06.09.
[10] Y. Wang, C. Zhao, D. Mei, G. Tang, L. Zhang, and D. Zhu, “Structural Design and Position Tracking of the Reconfigurable SCARA Robot by the Pre-Filter AFE PID Controller,” Applied Sciences, vol. 12, no. 3, p. 1626, Feb. 2022, doi: 10.3390/app12031626.
[11] H.-N. Nguyen, P.-N. Le, and H.-J. Kang, “A performance comparison of the full pose- and partial pose-based robot calibration for various types of robot manipulators,” Advances in Mechanical Engineering, vol. 13, no. 9, p. 168781402110477, Sep. 2021, doi: 10.1177/16878140211047754.
[12] T. Shu, S. Gharaaty, W. Xie, A. Joubair, and I. A. Bonev, “Dynamic Path Tracking of Industrial Robots With High Accuracy Using Photogrammetry Sensor,” IEEE/ASME Transactions on Mechatronics, vol. 23, no. 3, pp. 1159–1170, Jun. 2018, doi: 10.1109/TMECH.2018.2821600.
[13] Y. Zeng, W. Tian, D. Li, X. He, and W. Liao, “An error-similarity-based robot positional accuracy improvement method for a robotic drilling and riveting system,” The International Journal of Advanced Manufacturing Technology, vol. 88, no. 9–12, pp. 2745–2755, Feb. 2017, doi: 10.1007/s00170-016-8975-8.
[14] X. SHI, “Position and Attitude Measurement and Online Errors Compensation for KUKA Industrial Robots,” Journal of Mechanical Engineering, vol. 53, no. 8, p. 1, 2017, doi: 10.3901/JME.2017.08.001.
[15] H. X. Nguyen, H. Q. Cao, T. T. Nguyen, T. N.-C. Tran, H. N. Tran, and J. W. Jeon, “Improving Robot Precision Positioning Using a Neural Network Based on Levenberg Marquardt–APSO Algorithm,” IEEE Access, vol. 9, pp. 75415–75425, 2021, doi: 10.1109/ACCESS.2021.3082534.
[16] X. Li, H. Hu, and W. Ding, “Two Error Models for Calibrating SCARA Robots based on the MDH Model,” MATEC Web of Conferences, vol. 95, p. 08008, Feb. 2017, doi: 10.1051/matecconf/20179508008.
[17] Z. Wang, Y. Xu, Q. He, Z. Fang, G. Xu, and J. Fu, “Grasping pose estimation for SCARA robot based on deep learning of point cloud,” The International Journal of Advanced Manufacturing Technology, vol. 108, no. 4, pp. 1217–1231, May 2020, doi: 10.1007/s00170-020-05257-2.
[18] M. Švaco, B. Šekoranja, F. Šuligoj, and B. Jerbić, “Calibration of an Industrial Robot Using a Stereo Vision System,” Procedia Engineering, vol. 69, pp. 459–463, 2014, doi: 10.1016/j.proeng.2014.03.012.
[19] S. Hayati, “Robot arm geometric link parameter estimation,” in The 22nd IEEE Conference on Decision and Control, IEEE, 1983, pp. 1477–1483. doi: 10.1109/CDC.1983.269783.
[20] A. Nubiola and I. A. Bonev, “Absolute calibration of an ABB IRB 1600 robot using a laser tracker,” Robot Comput Integr Manuf, vol. 29, no. 1, pp. 236–245, Feb. 2013, doi: 10.1016/j.rcim.2012.06.004.
[21] A. Nubiola and I. A. Bonev, “Absolute robot calibration with a single telescoping ballbar,” Precision Engineering, vol. 38, no. 3, pp. 472–480, Jul. 2014, doi: 10.1016/j.precisioneng.2014.01.001.
[22] W. Zhenhua, X. Hui, C. Guodong, S. Rongchuan, and L. Sun, “A distance error based industrial robot kinematic calibration method,” Industrial Robot: An International Journal, vol. 41, no. 5, pp. 439–446, Aug. 2014, doi: 10.1108/IR-04-2014-0319.
[23] J. Zhou, H.-N. Nguyen, and H.-J. Kang, “Selecting Optimal Measurement Poses for Kinematic Calibration of Industrial Robots,” Advances in Mechanical Engineering, vol. 6, p. 291389, Jan. 2014, doi: 10.1155/2014/291389.
[24] W. Xiang and S. Yan, “Dynamic analysis of space robot manipulator considering clearance joint and parameter uncertainty: Modeling, analysis and quantification,” Acta Astronautica, vol. 169, pp. 158–169, Apr. 2020, doi: 10.1016/j.actaastro.2020.01.011.
[25] T. Tang, H. Luo, Y. Song, H. Fang, and J. Zhang, “Chebyshev inclusion function based interval kinetostatic modeling and parameter sensitivity analysis for Exechon-like parallel kinematic machines with parameter uncertainties,” Mechanism and Machine Theory, vol. 157, p. 104209, Mar. 2021, doi: 10.1016/j.mechmachtheory.2020.104209.
[26] Q. Meng, X. Lai, Z. Yan, C. Y. Su, and M. Wu, “Motion Planning and Adaptive Neural Tracking Control of an Uncertain Two-Link Rigid-Flexible Manipulator With Vibration Amplitude Constraint,” IEEE Transactions on Neural Networks and Learning Systems, vol. 33, no. 8, pp. 3814–3828, Aug. 2021, doi: 10.1109/TNNLS.2021.3054611.
[27] R. L. Truby, C. Della Santina, and D. Rus, “Distributed proprioception of 3D configuration in soft, sensorized robots via deep learning,” IEEE Robotics and Automation Letters, vol. 5, no. 2, pp. 3299–3306, Apr. 2020, doi: 10.1109/LRA.2020.2976320.
[28] J. Li, J. Wang, H. Peng, L. Zhang, Y. Hu, and H. Su, “Neural fuzzy approximation enhanced autonomous tracking control of the wheel-legged robot under uncertain physical interaction,” Neurocomputing, vol. 410, pp. 342–353, Oct. 2020, doi: 10.1016/j.neucom.2020.05.091.
[29] E. Z. Goh and T. Ali, “Robotic surgery: an evolution in practice,” Journal of Surgical Protocols and Research Methodologies, vol. 2022, no. 1, Jan. 2022, doi: 10.1093/jsprm/snac003.
[30] J. Klodmann et al., “An Introduction to Robotically Assisted Surgical Systems: Current Developments and Focus Areas of Research,” Current Robotics Reports, vol. 2, no. 3, pp. 321–332, Sep. 2021, doi: 10.1007/s43154-021-00064-3.

[31] C. Zhang and Z. Zhang, "Research on Joint Space Trajectory Planning of SCARA Robot Based on SimMechanics," in 2019 IEEE 3rd Information Technology, Networking, Electronic and Automation Control Conference (ITNEC), IEEE, Mar. 2019, pp. 1446–1450. doi: 10.1109/ITNEC.2019.8729547.
[32] Y. Tian et al., "RoboKeyGen: Robot Pose and Joint Angles Estimation via Diffusion-based 3D Keypoint Generation," Mar. 2024, [Online]. Available: http://arxiv.org/abs/2403.18259
[33] J. Li, L.-D. Yu, J.-Q. Sun, and H.-J. Xia, "A Kinematic Model for Parallel-Joint Coordinate Measuring Machine," Journal of Mechanisms and Robotics, vol. 5, no. 4, Nov. 2013, doi: 10.1115/1.4025121.
[34] Q. Zhao, J. Guo, and J. Hong, "System Kinematic Reliability Analysis for Robotic Manipulators Under Rectangular and Spherical Toler